

CIRCULATION PRODUCTION AND SHEDDING FROM VERTICAL AXIS WIND TURBINE BLADES UNDERGOING DYNAMIC STALL

Abel-John Buchner^{1,2,*}, Julio Soria^{2,3}, Alexander J. Smits^{1,2}

¹Department of Mechanical and Aerospace Engineering
Princeton University
Princeton NJ, USA

²Laboratory for Turbulence Research in Aerospace and Combustion (LTRAC)
Department of Mechanical and Aerospace Engineering
Monash University
Melbourne VIC, Australia

³Department of Aeronautical Engineering
King Abdulaziz University
Jeddah, Kingdom of Saudi Arabia

*abel-john.buchner@monash.edu

ABSTRACT

Dynamic stall of vertical axis wind turbine blades strongly affects the efficiency of vertical axis wind turbines, especially at low tip speed ratios. Here we report measurements using stereoscopic particle image velocimetry of the dynamic stall behaviour of such turbines, and discuss the factors affecting the evolution, strength, and timing of vortex shedding from the turbine blades. It is found that tip speed ratio alone is insufficient to describe the circulation production and vortex shedding behaviour, and a more complete scaling is proposed.

NOMENCLATURE LIST

c	Chord length of turbine blades
K_c	Dimensionless pitch rate
k	Turbulent kinetic energy
L	Length scale
R	Radius of vertical axis turbine
Re_c	Reynolds number
U	Velocity scale
U_∞	Freestream velocity
U_{rel}	Relative local velocity
α_{rel}	Angle of attack
Γ	Circulation
$\hat{\Gamma}$	Normalised circulation
θ	Azimuthal blade angle
λ	Tip speed ratio
ν	Kinematic viscosity
Ω	Rotation speed of vertical axis turbine

INTRODUCTION

Vertical axis wind turbines have the potential to surpass horizontal axis wind turbines for large-scale power generation (Dabiri, 2011; Sutherland *et al.*, 2012), but they have not been examined in similar detail, primarily due to the early success and current dominance of horizontal axis turbines in the wind power industry. The primary aerodynamic challenge facing vertical axis wind turbines is the tendency for the blades to dynamically stall. This dynamic stall behaviour is associated with the rapidly changing angle of attack experienced by the turbine blades during turbine rotation, and it may induce structural vibration, reduce efficiency, and increase noise production. Experimental studies at Sandia National Laboratories (Sutherland *et al.*, 2012) have examined the performance and power output of vertical axis wind turbine designs, but they have not explored in detail the conditions under which dynamic stall occurs in vertical axis wind turbines, and its severity, and the scaling behavior is not well understood. Here, we use Particle Image Velocimetry (PIV) experiments to investigate dynamic stall on vertical axis wind turbine blades in an effort to determine the correct scaling for the growth of the dynamic stall vortex and the effect of tip speed ratio and dimensionless pitch rate on the evolution of the dynamic stall vortex system.

NON-DIMENSIONAL PARAMETERS

The primary non-dimensional parameters are the tip speed ratio λ , the relative speed ratio U_{rel}/U_∞ , the relative angle of attack α_{rel} , the chord Reynolds number Re_c , and the dimensionless pitch rate K_c .

The tip speed ratio, λ , is defined as the ratio of the tangential velocity of the blade tip to the freestream velocity,

so that

$$\lambda = R\Omega/U_\infty.$$

The relative speed ratio is given by

$$U_{rel}^* = \frac{U_{rel}}{U_\infty} = \sqrt{1 + 2\lambda \cos \theta + \lambda^2},$$

where U_{rel} is the instantaneous relative velocity experienced by each blade, and the corresponding relative angle of attack is given by

$$\alpha_{rel} = \tan^{-1} \left(\frac{\sin \theta}{\lambda + \cos \theta} \right).$$

The variation of U_{rel}^* and α_{rel} during one cycle of rotation is illustrated in figure 1. We see that the amplitudes of the periodic oscillations in the local relative velocity and angle of attack diminish with increasing tip speed ratio. We expect, therefore, that at a sufficiently high tip speed ratio the flow over the blade would remain attached, and stall would not occur.

Since the oscillations in local relative velocity are centred about the tangential blade velocity, $R\Omega$, (figure 1(a)) this appears to be an appropriate choice for velocity scale when considering blade aerodynamics. The appropriate Reynolds number used in this experiment is therefore taken as the chord Reynolds number

$$Re_c = \frac{R\Omega c}{\nu}.$$

Given that the blade-relevant length and velocity scales in the case of vertical axis wind turbines are the chord length c , and the blade tangential velocity, $\lambda U_\infty = R\Omega$, the dimensionless pitch rate becomes

$$K_c = \frac{c}{2R},$$

which depends only on the geometry of the turbine. Note that the dimensionless pitch rate may be varied independently of the tip speed ratio.

EXPERIMENT

The 0.61×0.915 m cross-section wind tunnel at Princeton University was used to test a vertical axis wind turbine, of the H-type configuration, under a range of conditions. The test model has two NACA0015 blades, of span 450 mm, and is constructed of aluminium and carbon fibre. The turbine rotation is kept at a constant angular velocity and the tip speed ratio is varied by changing the freestream velocity. Three sets of blades were tested, with chord length $c = 50$ mm, 75 mm and 100 mm. The experimental setup is illustrated in figure 2.

Phase-locked stereoscopic PIV was performed in the region of the radially inwards facing surface of the turbine blade. Seeding was introduced into the freestream flow by an MDG brand clean nitrogen fed fog machine, producing

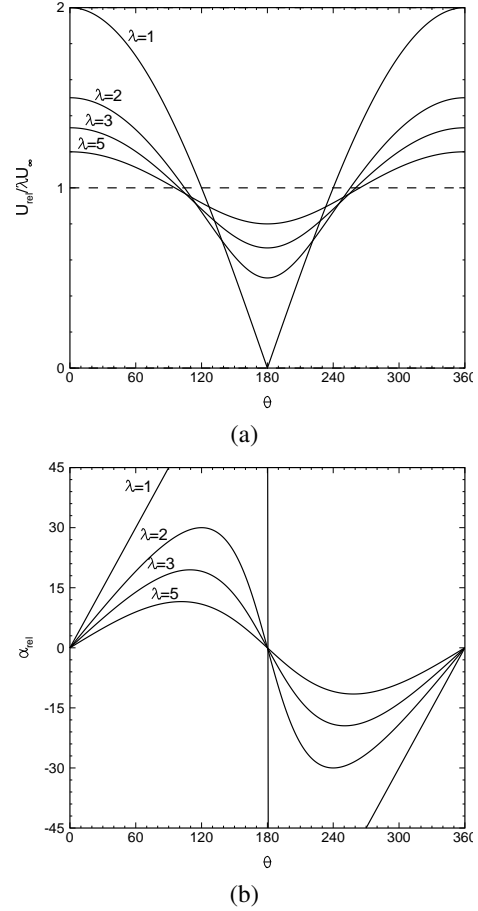


Figure 1. (a) Blade local relative velocity as a function of azimuthal position and tip speed ratio. Horizontal dashed line indicates tangential blade velocity, $R\Omega$. (b) Corresponding angle of attack.

a mean particle size of approximately $1 \mu\text{m}$. One thousand PIV image pairs were acquired at each of a range of azimuthal blade angles ($30^\circ \leq \theta \leq 165^\circ$), for each parametric condition.

Two sCMOS double shutter cameras were used, with a sensor resolution of 2560×2160 pixels. Each camera was fitted with a 50mm focal length lens, and was used to acquire particle displacement data over a region approximately 150×100 mm in size, corresponding to between one to three chord lengths, depending on the blade chord length, sufficient to capture the early-time development of dynamic stall on the turbine blades. The cameras were mounted on a turntable, centred on the turbine axis, to allow the rotation of the complete camera system to arbitrary azimuthal angles.

Data are presented for three chord-based Reynolds numbers, $Re_c = 50,000, 70,000,$ and $140,000$, at tip speed ratios varying from $\lambda = 1$ to $\lambda = 5$. The dimensionless pitching rate of the turbine blades was varied from $K_c = 0.10$ to $K_c = 0.20$. For each dimensionless pitch rate, the turbine angular velocity was held constant to ensure constant blade Reynolds number, while the freestream velocity was varied to effect changes in tip speed ratio. Table 1 lists the relevant parameters.

A multigrid cross-correlation (Soria, 1996) is per-

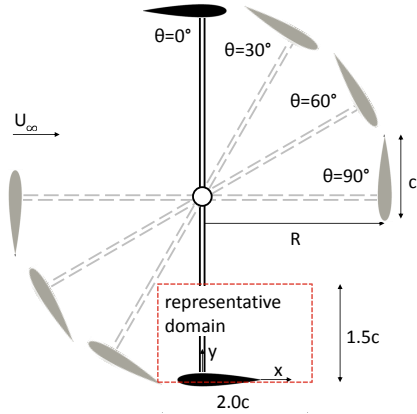
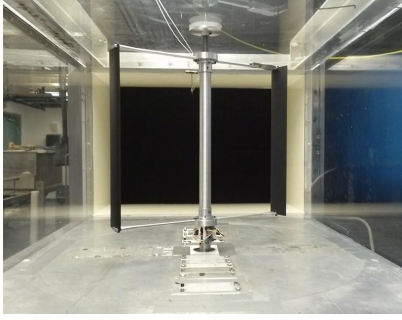


Figure 2. Wind turbine in wind tunnel test section (top), and schematic overview of turbine (as viewed from above), with representative measurement domain, coordinate system, and geometric parameters marked (bottom).

Table 1. Parameters of the experiment.

U_∞	4.5 – 22.6 m/s
c	0.05 – 0.10 m
Re	50,000 – 140,000
λ	1 – 5
K_c	0.10 – 0.20
θ	30° – 165°

formed on the PIV images, iterating from an initial window size of 64×64 pixels to a final size of 24×24 pixels. The final spatial resolution of the stereoscopic PIV measurement was approximately 0.7mm or $0.007c - 0.014c$ per vector. Prior to image cross-correlation, background scattered light and spurious reflections were removed from each image pair via a high pass filter and subtraction of the minimum intensity across the ensemble. Reflections from the turbine blade were masked. Application of a maximum displacement limit and a normalised local median filter (Westerweel & Scarano, 2005) to the raw displacement vectors resulted in the rejection of $\mathcal{O}(1\%)$ of the vectors. The velocities at the locations of the rejected vectors were interpolated from their nearest positively validated neighbours.

RESULTS AND DISCUSSION

Topology and turbulent fluctuation

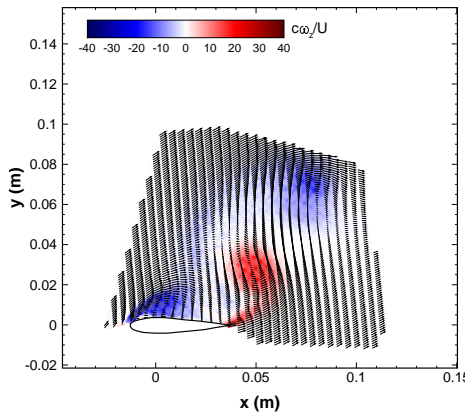
The early-time evolution of the stall depends strongly on tip speed ratio. Buchner *et al.* (2014) observed that in this early phase there exists an initial thickening of the boundary layer towards the blade’s trailing edge, accompanied by a small region of flow reversal, qualitatively similar to the incipient stages of a quasi-steady type stall. At high tip speed ratios no leading edge separation occurs, and no dynamic stall vortex forms, and the blade remains largely unstalled until the upper surface boundary layer reattaches as the turbine blade recedes from the oncoming flow and the angle of attack is again reduced.

At lower tip speed ratios, the turbine blades exhibit dynamic stall behaviour, with the boundary layer separating at the leading edge, forming a small vortex attached to the upper surface of the airfoil. As the stall progresses, the leading edge dynamic stall vortex grows significantly in spatial extent and moves away from the surface of the blade. The interaction of the leading edge vortex with the no-slip boundary condition at the blade’s upper surface induces a region that has a circulation opposite in sign to the primary leading edge vortex, located between the primary vortex and the blade surface. As the angle of attack increases further, a trailing edge vortex develops, which interacts with the leading edge vortex to change its size, shape, and motion.

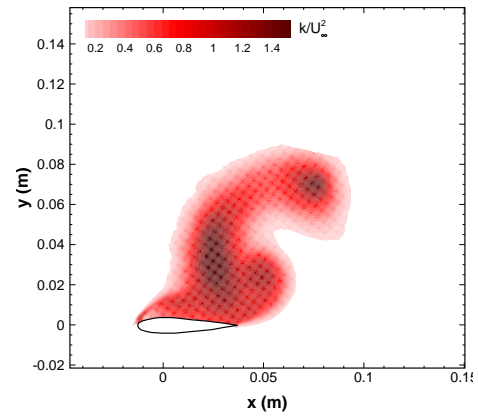
In addition to the effect of tip speed ratio as documented by Buchner *et al.* (2014), the effect of dimensionless pitch rate on the dynamic stall evolution is also important. Figure 3 illustrates the dynamic stall behaviour at $\theta = 105^\circ$ for a tip speed ratio of $\lambda = 2$. The three figures relate, from top to bottom, to $K_c = 0.10, 0.15,$ and 0.20 , and show that the primary effect of increasing pitch rate is to diminish the spatial growth of the leading edge vortex, thereby reducing and delaying the interaction between leading and trailing edge vorticity. Mutual induction between the leading and trailing edge vortices tends to pull the leading edge vortex away from the blade, leading to the topological differences seen in figure 3(a), where the leading edge vortex has shed early and convected significantly aft, and a second stall vortex is seen to be forming.

The Reynolds number of the flow over the turbine blades is such that the unsteady separating flow is of a highly turbulent nature. Referring to figure 4, it is possible to observe the spatial distribution of turbulent fluctuations in the dynamic stall vortex system for the same conditions as those in figure 3. The magnitude of the turbulent kinetic energy appears to scale across pitching rates and tip speed ratios with the square of the freestream velocity, and the distributions presented here are normalised by this value. The highest pitching rate case presented here, $K_c = 0.20$, (figure 4(c)) displays a smaller leading edge vortex core than the lower pitch rate cases, with intense fluctuations in the core. At the other end of the parameter range, the $K_c = 0.10$ case, the strikingly different topology seen in figure 3(a) is reflected in the turbulent kinetic energy distribution (figure 4(a)). As with the higher pitching rate cases, turbulent fluctuations are associated with vortex cores, but the region of interaction between the leading and trailing edge vortices, where the leading edge vortex is being stretched away from the blade, exhibits significant fluctuation also.

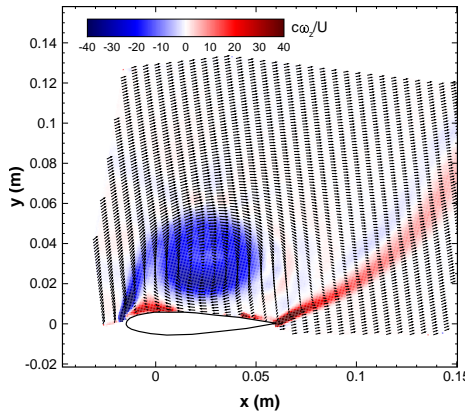
The effect of the leading–trailing edge vortex interaction may be quantified by tracking the core of the leading edge vortex as it convects away from the turbine blade. The path taken by the leading edge vortex at $\lambda = 1$ is plotted in



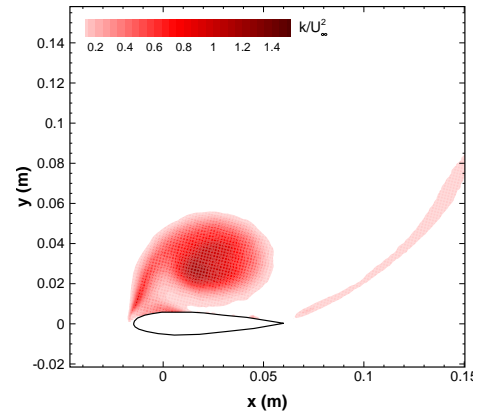
(a)



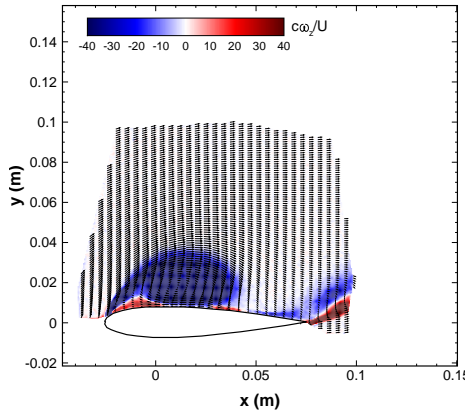
(a)



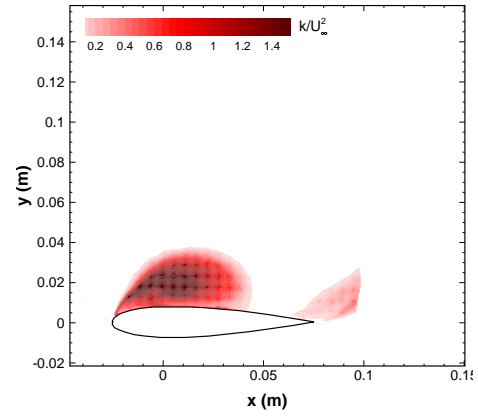
(b)



(b)



(c)



(c)

Figure 3. Phase-averaged vorticity contours and vector fields in the vicinity of a NACA0015 vertical axis wind turbine blade, at $Re_c = 70,000$, $\theta = 105^\circ$, $\lambda = 2$. (a) $K_c = 0.10$, (b) $K_c = 0.15$, (c) $K_c = 0.20$.

Figure 4. Turbulent kinetic energy k/U_∞^2 at $Re_c = 70,000$, $\theta = 105^\circ$, $\lambda = 2$. (a) $K_c = 0.10$, (b) $K_c = 0.15$, (c) $K_c = 0.20$.

figure 5 as the dimensionless pitch rate varies. Post-stall, as the blade recedes from the oncoming freestream, one might expect at this tip speed ratio that the shed vortices should convect downstream at about the same streamwise position as the blade. Indeed, this is observed in the case of $K_c = 0.15$ and $K_c = 0.20$. The leading edge dynamic stall vortex initially grows close to the plate's upper surface before moving away in close to a normal direction to the chord line. As dimensionless pitch rate is decreased however, the

leading edge vortex is instead seen to travel rapidly aft of the blade, due to increased interaction with the trailing edge vortices.

Stall angle

The azimuthal angle at which leading edge dynamic stall vortex first appears, θ_{stall} , is plotted against tip speed ratio in figure 6(a). We see that the primary effect of increasing tip speed ratio is to delay the angle at which stall is

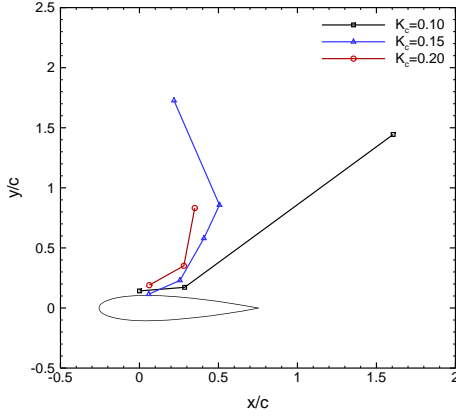


Figure 5. Motion paths of the leading edge vortex, for $\lambda = 1$, showing variation with dimensionless pitch rate.

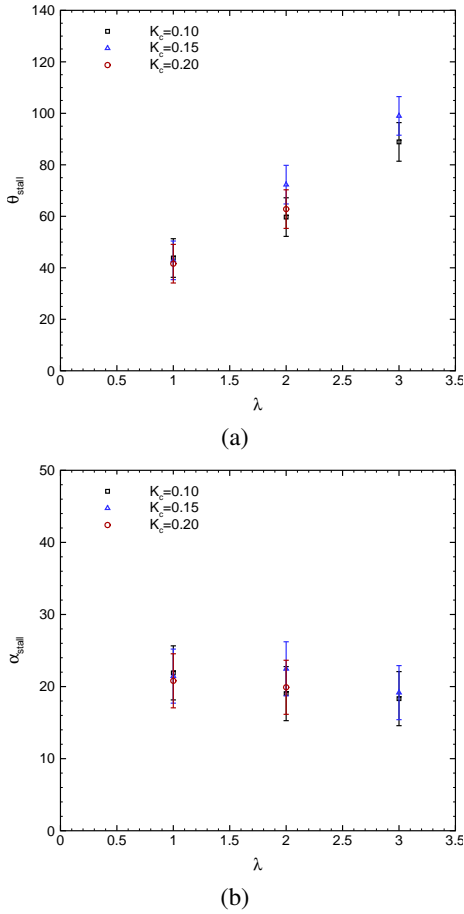


Figure 6. Stall angle (angle at which leading edge vortex first appears) in degrees. (a) Azimuthal stall angle; (b) relative angle of attack at stall.

initiated. This observation is consistent with the inferences made from the stall topology. The data also suggest that the dimensionless pitching rate, K_c has minimal or no effect on the initial stall angle of the blade.

Figure 6(b) shows the relative angle of attack, α_{stall} , at which stall begins. Within the margin of error of the measurement, the angle of attack of dynamic stall appears in-

variant with both tip speed ratio and dimensionless pitch rate, at a constant value between 18 and 23 degrees. At comparable Reynolds numbers, the static stall angle for a NACA0015 airfoil is approximately 10 degrees.

Scaling the circulation production

The phase-averaged circulation in the leading edge dynamic stall vortex is shown in figure 7(a) as a function of θ for $K_c = 0.15$, and tip speed ratio $\lambda = 1, 2$, and 3. It is clear that, consistent with observed stall onset delay, the production of circulation is also significantly delayed as tip speed ratio is increased. This trend holds true for $K_c = 0.10$ and $K_c = 0.20$ also.

Figure 7(b) illustrates the circulation production trend with dimensionless pitch rate at $\lambda = 2$. A weak dependence of the rate of circulation production post-stall on the pitch rate can be seen. Higher pitch rates tend to reduce the rate at which circulation is shed into the leading edge vortex.

It appears that the relevant velocity scale for the production of circulation from the turbine blades' leading edge is the freestream velocity. Normalising the leading edge vortex circulation by the chord length and freestream velocity,

$$\hat{\Gamma} = \frac{\Gamma}{cU_\infty},$$

and subtracting the stall angle from the azimuthal angle, collapses the data at any given tip speed ratio. This scaling does not however account for variation in pitch rate. To adjust for pitch rate effects on circulation production rate, the time-scale must also be modified.

All circulation shed post-stall from the leading edge has its genesis in the shear-layer at the leading edge of the blade, where the velocity differential is $\mathcal{O}(U_\infty)$. Per unit length along the blade's surface, the circulation produced here might scale according to

$$\Delta\Gamma \sim U_\infty \Delta x \sim U_\infty R \Delta\theta$$

since Δx equates to the tangential distance travelled by the blade, $R\Delta\theta$. We expect, therefore, that

$$\hat{\Gamma} = \frac{\Gamma}{cU_\infty} \sim \frac{R}{c} \int_{\theta_{stall}}^{\theta} d\theta$$

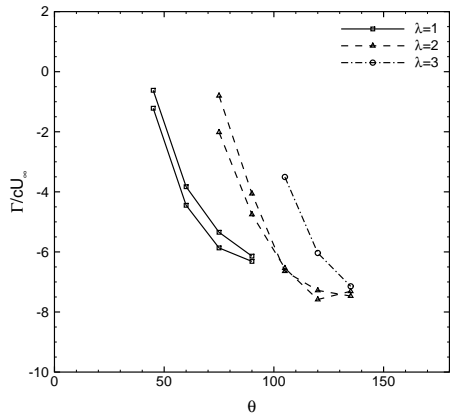
so that

$$\hat{\Gamma} = \frac{\Gamma}{cU_\infty} \sim \frac{1}{K_c} (\theta - \theta_{stall}).$$

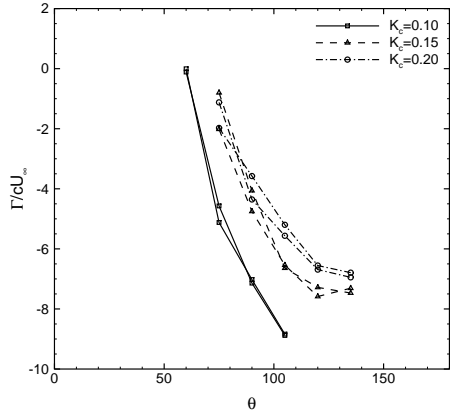
Figure 7(c) demonstrates that the data agree well with this basic scaling, and although the relationship is not linear it seems clear that the production of circulation at the leading edge is governed by the post-stall distance travelled by the blade, about the circumference of the turbine.

CONCLUDING REMARKS

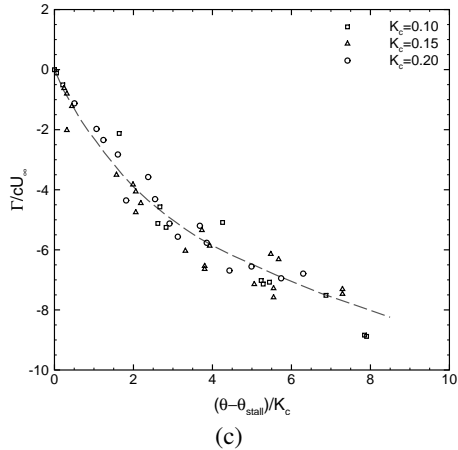
It has been found that both the rate of accumulation of circulation in the leading edge dynamic stall vortex, and the



(a)



(b)



(c)

Figure 7. Phase-averaged normalised circulation in the dynamic stall vortex. (a) Variation with λ at $K_c = 0.15$, (b) variation with K_c at $\lambda = 2$, and (c) collapse with scaling of production rate based on dimensionless pitch rate.

azimuthal position of the initial formation the stall vortex depend on multiple parameters.

Increasing tip speed ratio tends to delay the azimuthal angle at which a dynamic stall vortex forms, and to decrease the total circulation ultimately shed into the dynamic stall vortex. These observations are consistent with the increased dominance at high tip speed ratios of the tangential velocity of the blade over the freestream velocity component, and thus the smaller variation in angle of attack at these tip speed ratios. At a tip speed ratio of approximately 3 to 3.5, no leading edge separation occurs and no dynamic stall vortex forms.

Changes in the dimensionless pitching rate significantly affect the stall topology. The spatial extent of the leading edge vortex varies inversely with pitching rate, with greater spatial growth of the dynamic stall vortex at lower pitch rates forcing a stronger interaction between the leading and trailing edge vortices, inducing the leading edge vortex to pinch off from the blade at an earlier azimuthal position, and a second leading edge stall vortex to form. This phenomenon has a significant effect on the overall velocity field and is an important consideration in the prediction of the effect of dynamic stall on the production of blade forces.

The total circulation shed in the dynamic stall process at the leading edge was found to scale with the chord length of the turbine blades and the freestream velocity, but an adjustment to the time-scale over which this occurs is necessary to account for pitch rate effects on the circulation production rate. The rate of circulation shedding at the leading edge was found to scale with the post-stall azimuthal distance travelled by the blade. The circulation production and shedding behaviour is consistent across the range of Reynolds numbers tested here.

ACKNOWLEDGEMENTS

This research is supported by the Australian-American Fulbright Commission and the Princeton University's Andlinger Center for Energy and the Environment.

REFERENCES

- Buchner, A.-J., Smits, A. J. & Soria, J. 2014 Scaling of vertical axis wind turbine dynamic stall. *19th Australasian Fluid Mechanics Conference, Melbourne, Australia*.
- Dabiri, J. O. 2011 Potential order-of-magnitude enhancement of wind farm power density via counter-rotating vertical axis wind turbine arrays. *Journal of Renewable and Sustainable Energy* **3**.
- Soria, J. 1996 An investigation of the near wake of a circular cylinder using a video-based digital cross-correlation particle image velocimetry technique. *Experimental Thermal and Fluid Science* **12** (2), 221–233.
- Sutherland, H. J., Berg, D. E. & Ashwill, T. D. 2012 A retrospective of vawt technology. *Sandia Report SAND2012-0304*.
- Westerweel, J. & Scarano, F. 2005 Universal outlier detection for piv data. *Experiments in Fluids* **39** (6), 1096–1100.